OXFORD

Transportation Safety and Environment, 2025, **7**: tdaf060

DOI: 10.1093/tse/tdaf060
Research Article

Study and testing of wheelset wheel-flat identification features through axle-box vibration measurements

Arianna Cavallo [1,*], Stefano Cii [1], Gisella Tomasini [1], Francesco Castelli-Dezza [1], Steven Cervello[2] and Daniele Regazzi[2]

[1]Department of Mechanical Engineering, Politecnico di Milano, Via Privata Giuseppe La Masa, 20156 Milan, MI, Italy;
[2]Railway Division, Lucchini RS S.p.A., Via G. Paglia, 24065 Lovere, BG, Italy.
*Corresponding author. E-mail: arianna.cavallo@polimi.it

Abstract

Early detection of wheelset defects is essential for ensuring railway safety. Wheelset condition monitoring can provide continuous information about the health of the system, thus avoiding time-consuming and expensive operations such as periodic inspections. This work deals with the study of railway wheelset wheel-flat identification features based on vibration signals from axle-box measurements. The aim is to obtain a simple and straightforward solution that can be easily implemented on a complete autonomous on-board sensor for wheelset defect prediction. Numerical simulations, by coupling a multi-body model of a coach with a new approximation of a wheel-flat model, were run in order to estimate the nature of the problem and the technical acquisition characteristics needed for a sensor node to be installed on real trains. Then, experimental campaigns were carried out on a wheelset test bench with defects artificially created to validate the presented methodology based on time domain feature extraction. A signal processing technique, which does not require the aid of any other hardware to obtain the revolution speed, is proposed. The methodology allows clear detection of wheel flats starting from 30 mm, especially at lower speeds. Even when considering the influence of wear, high defect conditions remain easily distinguishable.

Keywords: railway wheelset; wheel-flat; axle-box; vibration measurements; full-scale experimental tests; sensor node

Highlights

- A method based on vertical axle-box accelerations has been developed to identify wheel flats based on time domain features. The method is suitable for implementation on microcontrollers, does not need any other hardware tool (e.g., GPS) and leads to a substantial data reduction, making it extremely valid for data transmission from on-board sensors to online clouds.
- Multi-body simulations of a railway coach have been performed in the absence and presence of a wheel-flat, with the aim of estimating the sampling parameters for an on-board sensor, specifically the minimum sampling frequency and full scale.
- Experimental tests have been performed on a full-scale test bench, where wheel flats of growing size have been artificially reproduced on a wheelset. Axle-box accelerations have been sampled at three velocities. This test allows the sampling of acceleration data where the actual profile of a peak generated by a wheel-flat is captured.
- The influence of wear has been verified by performing tests where the wheelset has been left running on the test bench for several kilometres.

1. Introduction

Wheelset defects include tread anomalies such as wheel out-of-roundness (OOR), defined as any deviation from a perfectly circular shape. These can be periodic (e.g., polygonal wheels), random or discrete (e.g., wheel flats or clusters from rolling contact fatigue) [1]. In addition, axle defects may also arise, as cracks. Wheelset defects represent crucial elements when discussing railway safety, as they can lead to severe disturbances and undesired failures.

In Europe, while each rolling stock operator may have its own regulations and logistic plans for wheelset monitoring, general guidelines from the *Verband der Güterwagenhalter in Deutschland* (VPI) are widely followed. For instance, VPI 03 and VPI 04 provide maintenance directions for freight trains' railway wheelsets, ranging from simple visual inspections (IS0) to comprehensive axle replacements (IS3) [2]. The Italian company Mercitalia Intermodal performs IS1 maintenance after 300,000 km and IS2 maintenance after 600,000 km [3]. Additionally, it conducts visual inspections of each bogie after every trip, leading to numerous unexpected inspections, with 10% identifying type 1.3 of wheel defects [4], i.e., defects on the tyre or corresponding part of the solid wheel. Visual inspections are costly and time-consuming, especially for long freight trains. Defective wheelsets require the separation and dismantling of cars, causing further delays and financial losses. In this regard, predictive maintenance aims to minimize failures and costs without impacting productivity [5]. Unlike traditional maintenance based on routine controls, predictive maintenance schedules tasks as needed by the equipment [6, 7]. For wheelset defects in freight trains, early defect detection can support or even replace visual inspections, extending wheelset service life by identifying minor defects early, also decreasing the material removal at each re-profiling.

Received: April 14, 2025. **Revised:** September 17, 2025. **Accepted:** September 25, 2025
© The Author(s) 2025. Published by Oxford University Press on behalf of Central South University Press. This is an Open Access article distributed under the terms of the Creative Commons Attribution License (https://creativecommons.org/licenses/by/4.0/), which permits unrestricted reuse, distribution, and reproduction in any medium, provided the original work is properly cited.

Downloaded from https://academic.oup.com/tse/article/7/4/tdaf060/8362716 by Dipartimento di Elettronica/Informazione user on 06 March 2026

Thus, research in railway vehicle condition monitoring has seen rapid growth in recent years, particularly in the development of defect identification techniques.

Monitoring of railway vehicles can happen through sensors installed on the railway infrastructure, e.g., wayside monitoring, or through sensors placed on the vehicle itself, e.g., on-board monitoring. For the former, a comprehensive review of methods for wheelset defects monitoring can be found in Ref. [8]. The convenience of the wayside technique relies on the possibility of employing a single set of sensors to monitor a great number of vehicles that are crossing that point in the railway line. At the same time, these sensors rely on algorithms not properly tuned for the specific vehicle and cannot perform continuous analysis.

Exhaustive research is now being carried out focusing on the topic of on-board wheelset condition monitoring. In Refs. [9, 10], different approaches of on-board wheelset condition monitoring were investigated, including magnetic, ultrasonic, acoustic and vibrational techniques. As pointed out in a recent comprehensive review by Ye et al. [11] on wheelset fault diagnosis, acceleration-based methods have become the most explored path in the scientific community, due to the ease of installation, the accelerometers' low cost and the significant improvements in the signal processing techniques. Among the vibrational detection approaches available, some of them concern the employment of axle-box acceleration, i.e., ABA, signals: these can indeed be considered quite reliable, as they gather vibrational data very close to the possible source of the problem.

The focus of this work is the development of an algorithm, based on time domain features, for the identification of a specific wheelset defect, wheel-flat, by means of on-board vertical ABA measurements. The objective is to develop a solution that can be seamlessly integrated into an AB on-board sensor, specifically designed for micro-controller implementation. This solution aims to achieve low power consumption and minimal memory storage requirements and to facilitate easy and compact hardware assembly. Consequently, the study also focuses on identifying and defining the essential requirements that an on-board sensor must have to effectively employ the proposed algorithm.

Wheel-flat is a wheel geometry profile defect caused by wheel locking during the braking process and successive sliding on the rail, or by low adhesion to the rail for environmental outliers such as leaves or snow [12]. It is one of the most common local surface defects and with time can cause further degradation of wheels, bearings and suspensions. Furthermore, it can produce high levels of noise [13], impact loading of the track [14, 15] and worsen wheel polygonization [16]. Finally, the sliding and subsequent renewed rolling of the wheel will cause a temperature rise, followed by rapid cooling. The latter will lead to the formation of brittle martensite around the flat, generating high forces and stresses on the vehicle components and possibly also leading to the initiation of fatigue cracks [17, 18]. As a consequence, early identification of wheel-flat becomes of crucial importance.

The latter can be achieved in different ways, such as ultrasonically [19] or through the employment of Fiber Bragg Grating [20], but is often done by ABA measurements: indeed, the presence of a wheel-flat induces in the vertical acceleration a peak value at every complete rotation of the wheel in correspondence to the angle of rotation for which the wheel-flat is passing through the contact point between wheel and rail.

Time domain and frequency domain identification approaches can be found in the literature. Liang et al. [21] developed a simplified mathematical model and simulation of wheel-flat and rail surface defects, which they validated against scaled roller rig experiments, including ABA signals. Time-frequency techniques were tested (as Short Time Fourier Transform, Wigner-Ville Transform and Wavelet Transform), coupled with time domain parameters: the faulty signals were detected but only at very low speed, a maximum of 7 km/h, and for a single case of very low dimension wheel-flat of 2 mm. The same roller rig was employed later on in Ref. [22]: adaptive noise cancelling proved to be an ally in detecting faults, especially at high speed, when applied in time–frequency signal processing techniques.

Chen et al. [23] proved how a two-level adaptive chirp mode decomposition method can detect wheel-flat under variable-speed conditions, showing the algorithm's potential on an experimental model vehicle. In Ref. [24], empirical mode decomposition was applied to wheel-flat detection and proved effective even on non-stationary signals. However, its high computational cost poses challenges for on-board implementation. In regard to this, time-domain detection methods can be more advantageous. In addition, the algorithm was validated on a test rig employing a rubber block to simulate the impact of a wheel-flat, with no guarantee it would be as effective with an actual defect. Similarly, Li et al. [25] proposed an adaptive multiscale morphological filter for wheel-flat diagnosis, also validated on a roller rig using a rubber block to mimic impulsive forces. As the authors noted, the impulsive features generated by a real wheel-flat and those produced by a rubber block may not be entirely equivalent.

It is important to note that many of the existing algorithms for wheel-flat identification require a synchronous sample of the acceleration signal, obtained by means of a direct measure of the vehicle speed, to work in the angular domain. This can be obtained with an encoder, the implementation of which is not straightforward for an on-board solution.

Bosso et al. [26] used vertical ABA and analysed it in the time domain to detect wheel flats. The algorithm was tested on numerical simulations and experimental tests. The limitation is that an encoder was used to determine the angular position of the wheelset and the algorithm was designed to work in a nearly constant speed condition. Furthermore, the algorithm was tested on a Y25 freight train and validated with a maximum admissible speed of 90 km/h. Shim et al. [27] combined order analysis first with cepstral analysis, then with cross-correlation analysis, to evaluate the wheel-flat signal, even under variable speed conditions. Also in this study, the presence of an encoder or a generic speed sensor is taken for granted. Bernal et al. [28] developed an interesting study for wheel-flat identification through the employment of analogue signal processing techniques. Their algorithm was validated through an experimental campaign on a 1:4 model test rig with an artificially ground 40 mm defect. To be able to work in a wide range of speeds, the authors indicated the need for a GPS solution. In Refs. [29, 30], wheel flats on railway vehicles were detected through the angular domain synchronous averaging, i.e., ADSA, method, which can also handle the non-stationary vibration process. The method was experimentally validated with a single 50 mm long defect (only 10 mm shorter than the limit value [31]) and for very low velocity, only 30 km/h, quite far from the cruise velocity of freight or high-speed trains. In addition, even though the algorithm could be easily implemented, the authors indicate the need for a tachometer for measuring the rotational velocity of the wheel. In conclusion, machine-learning approaches [32, 33], or deep-learning algorithms, [34–36], are also applied for this topic.

The methodology developed in this work for wheel-flat identification relies on time-domain feature extraction and finds itself, according to the definition given in Ref. [11], among the clas-

Downloaded from https://academic.oup.com/tse/article/7/4/tdaf060/8362716 by Dipartimento di Elettronica/Informazione user on 06 March 2026

sical signal processing methods. The problem was studied starting from numerical simulations, where vertical ABA vibration signal characteristics were quantified, defining the full scale and the minimum sampling frequency that an on-board sensor would require to be able to detect such a defect. The algorithm was validated through experimental tests on the Lucchini RS BU300 full-scale test bench, testing increasing defect dimensions at three velocities, coupled with the wearing phenomenon, which naturally affects real-life working wheelsets. This approach presents the following innovations. It is able to derive wheelset rotational speed directly from acceleration measurements, bypassing the need for an encoder measurement, which is essential for an on-board ABA sensor. This is achieved through the implementation of cepstral analysis, which is performed by reversing the methodology proposed by Baasch et al. [37], aimed at the identification of the wheel radius from the previously obtained speed. Furthermore, thanks to the employment of a full-scale test rig, the authors were able to accurately reproduce the time profile of the impulse associated with wheel-flat presence, verifying the presented algorithm on various defect sizes and testing the effect of their presence at three velocities. In addition, the coupling effect with the wear, a naturally occurring phenomenon in field scenarios, was studied.

2. Numerical simulations

Defects such as the wheel-flat introduce irregularities in the wheelset operational behaviour, thus changing their dynamic response. The controlled environment of numerical simulations enabled a first estimation of the relationship between wheel-flat presence and the resulting vibration patterns. By increasing defect size and running velocity, the trend of time-domain features computed on ABA signals is observed, once vertical, lateral and longitudinal acceleration signals have been extracted. An estimation of the minimum requirements (in terms of sampling frequency and full scale) needed by an on-board sensor to correctly sample ABA signals in the presence of a wheel-flat is performed.

The numerical simulations are carried out by means of a mathematical model developed by the railway dynamics research group of the Department of Mechanical Engineering of the Politecnico di Milano. The mentioned model is a complete multi-body model of a coach, aimed at simulating a vehicle running on a railway line. The model is able to describe very accurately the vehicle dynamics and the wheel–rail interaction, taking into account the track deformability. The wheel-flat is introduced as a change in the nominal shape of the wheel profile.

2.1. Modelling

The mathematical model employed for the train track interactions consists of three parts: a multi-body model of the rail vehicle, a simplified/complete model of the track and a model of wheel/rail contact. More details about the modelling approach can be found in Ref. [38]. The model is based on a multi-body schematization of the trainset, enabling the analysis of the non-stationary running behaviour in the tangent track and curve of a single vehicle. The vehicle system includes three elementary modules.

- The car body, modelled as a single rigid body, as the effect of its own flexibility on wheelset acceleration is negligible.
- The bogie assembly, modelled as a rigid frame connected by primary suspension to two wheelsets, modelled as deformable bodies. The latter are expected to have a relevant effect on the high-frequency component of wheel/rail contact forces.
- The secondary suspension, modelled as a combination of lumped parameter linear and non-linear visco-elastic elements.

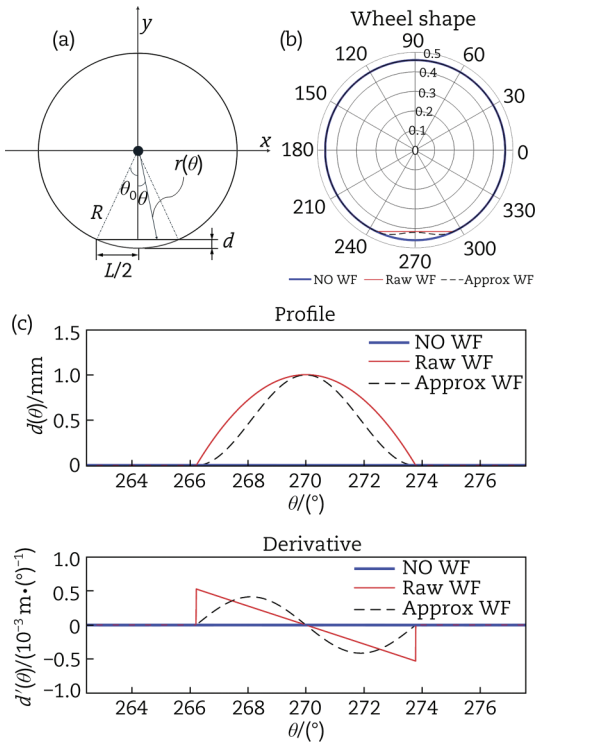

Fig. 1. (a) Raw wheel-flat geometry parameters [19], (b) no wheel-flat, raw wheel-flat, approximated wheel-flat comparison, and (c) deviation from the ideal circular profile in the upper plot and derivative of the profile in the lower plot

The number of degrees of freedom for the complete vehicle is 63.

Track flexibility is accounted for through a finite element scheme, in which the rails and sleepers are modelled by Euler-Bernoulli beam elements: two beam elements are used to model each sleeper span on each rail and four beam elements are used to model each sleeper. The rail pads and fastening devices are modelled as linear visco-elastic elements connecting the rails to the sleepers. The ballast is represented as a series of lumped masses—one beneath each sleeper—connected to both the sleeper and the ground by two visco-elastic layers acting in the vertical and lateral directions. The finite element model is three-dimensional and considers the vertical and lateral motion of the track, whereas the longitudinal displacements are not considered in the simulation. In this work, the finite element model consists of 500 sleeper spans, corresponding to a track length of 300 m.

The model of wheel–rail contact used to reproduce the dynamic coupling between the vehicle and the track is the pre-tabulated, multi-Hertzian one [39]. The only condition dealt with in this work is the simulation of tangent track running of the vehicle and the assumption is made that one single contact point occurs between each wheel and the rail.

The wheel-flat defect modelling relies on a further approximation of the wheel-flat raw modelling described in Ref. [19], the scheme of which can be seen in Fig. 1(a). The raw wheel-flat model is expressed through Eq. (1), where $d(\theta)$ is the defect amplitude

Downloaded from https://academic.oup.com/tse/article/7/4/tdaf060/8362716 by Dipartimento di Elettronica/Informazione user on 06 March 2026

and θ is the angular position, positive if taken counter-clockwise starting from the positive direction of x-axis. $r(\theta)$ is the real radius of the wheel with the defect, expressed by Eq. (2).

$$d(\theta) = R - r(\theta) \tag{1}$$

$$r(\theta) = \begin{cases} R, & \theta < 3\pi/2 - \theta_0 \\ R\cos\theta_0/\sin\theta & 3\pi/2 - \theta_0 < \theta < 3\pi/2 + \theta_0 \\ R, & \theta > 3\pi/2 + \theta_0 \end{cases} \tag{2}$$

Since the raw wheel-flat model presents discontinuities in the first derivative, a more physical model has been adopted. The latter approximates the raw geometry with a smooth sinusoidal function and represents a rounded flat. Fig. 1(b) shows a comparison between the raw wheel-flat model and the sinusoidal function model. In the figure, the defect depth is 1 mm, amplified by a factor of 40 for visualization purposes. Fig. 1(c) shows a comparison, in terms of deviation from the nominal circular profile and its derivative, between the raw wheel-flat model and the approximated one. Fig. 1(c) curves are related to a 1 mm deep and 60 mm long defect. The sinusoidal approximation is primarily intended to regularize the defect geometry for numerical simulations, ensuring continuity and smooth derivatives, preserving the overall defect depth and angular extent, and eliminating the abrupt slope changes at the defect edges.

The simulations are based on two parameters:

- d, depth of the defect, computed as the maximum of the $d(\theta)$ function previously described;
- L, longitudinal extension of the defect, directly related to the angular sector θ through the formulation $L = 2R\theta$.

The constraint that links d and L to the angular sector θ maintains exactly the same ratio d/L in the definition of 'raw wheel-flat', while this constraint is removed in the simulations performed letting L and d be freely chosen around the nominal ratio d/L.

2.2. Results

Numerical simulations relied on the following parameters.

- Vehicle: ETR1000 full coach.
- Track profile: UIC 60, standard irregularity according to report ORE B 176 [40].
- Speed (km/h): 100, 200, 300.

A combination of wheel-flat length and height is run: the same defects have also been reproduced in the full-scale tests performed on the Lucchini RS test bench (See Section 3.1 for further information). It is important to stress that it is possible to choose length and height independently from each other due to the local cosine function adopted for modelling the wheel-flat (while, in the raw wheel-flat definition, they should be strictly correlated). The defect is applied only to the left wheel; the right wheel has a standard profile. Table 1 lists the names and dimensions of said defects.

As expected, the results of the multi-body simulations show the presence of peaks in the vertical acceleration time history with a periodicity equal to the $1\times Rev$, i.e., first harmonic revolution, of the wheel Fig. 2(a).

Table 2 summarizes the simulation results. It is worth underlining that WF2 data results are omitted since the corresponding experimental data suffered from damages due to a faulty cable. In the presence of a wheel-flat, a significant increment of the crest factor (CF) value is observed, with a strong independence from speed since, as the latter increases, both the peak value and the root mean square (RMS) grow proportionally. The highest peak values are obtained for WF4 but also for WF1, near 30g. Probably this is due to the sharper profile of the wheel radius derivative. The mathematical model adopted for simulations uses an infinitely rigid wheel profile and does not allow for any local deformation, a thing that would instead happen in a real-case scenario, decreasing the peak values caused by wheel-flat, especially for small defects.

Table 1. Numerical simulations of wheel-flat (WF) defects, with dimensions

Defect name	Length (mm)	Height (mm)
WF1	10	2×10^{-2}
WF2	30	2×10^{-2}
WF3	30	5×10^{-2}
WF4	30	8×10^{-2}
WF5	60	8×10^{-2}

The maximum peak value and the peak duration are computed to set minimum requirements for an on-board measurement sensor, in terms of full scale and sampling frequency f_{samp}, respectively. The peak duration is computed as the time interval between the two half-power peaks (HPPs), consecutive values, to guarantee a sampling frequency high enough to get at least one point inside this interval. The minimum sampling frequency is therefore computed through Eq. (3).

$$f_{samp\,min} = \frac{1}{peak_{dt}} \tag{3}$$

The results of Table 2 indicate very high values of required sampling frequency, such as 25 kHz for WF1 on a vehicle running at 300 km/h, which would be incompatible for the implementation of an on-board sensor, due to the amount of data that would be generated. Thus, the downsampling procedure is adopted, to simulate the effect of digital acquisition and ultimately define the minimum sampling frequency that well describes the signal with no loss of information about the peaks. To do this, a statistical approach is employed where the probability P_{tot} of getting at least one peak in a certain time window of length T_{tot} is described by Eq. (4), where p is the probability to place at least one sampled point in the time interval of the peak and it is computed through Eq. (5).

$$P_{tot} = 1 - (1-p)^{\frac{T_{tot}}{T_{1\times Rev}}} \tag{4}$$

$$p = \frac{peak_{dt}}{dt} \tag{5}$$

By considering different combinations of T_{tot} and f_{samp}, the ones that guarantee a probability $P_{tot} > 99.9\%$ are:

- $f_{samp} = 1{,}600$ Hz and $T_{tot} = 5$ s;
- $f_{samp} = 800$ Hz and $T_{tot} = 10$ s.

Fig. 2 (b) shows an example of downsampling at 800 Hz with a comparison with the original signal: even though some peaks are lost or partially sampled, others are correctly described.

3. Experimental tests

The experimental tests are designed to validate, in a full-scale setting, a wheel-flat identification algorithm based on time-domain features computation on $1\times Rev$ time windows. The experimental tests were conducted on the BU300 roller rig test bench, which is located in Lovere (BG), Italy, at the industrial facility of Lucchini

Downloaded from https://academic.oup.com/tse/article/7/4/tdaf060/8362716 by Dipartimento di Elettronica/Informazione user on 06 March 2026

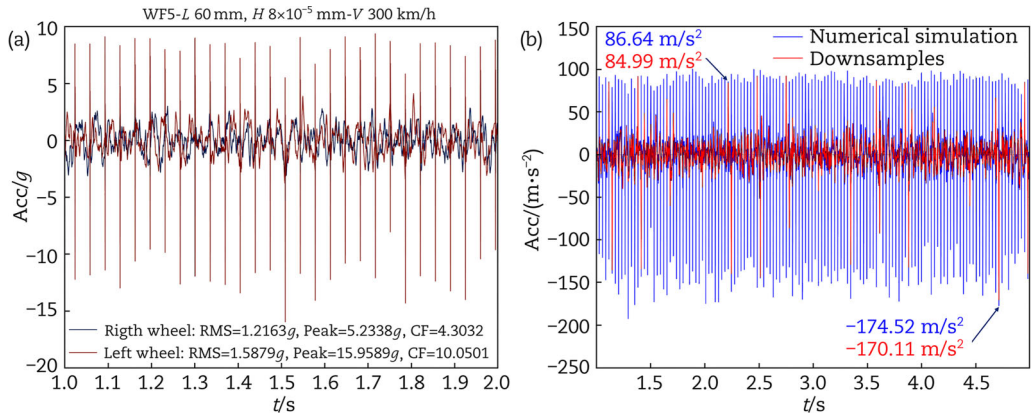

Fig. 2. Numerical simulations: (a) vertical 1 s ABA time history at 300 km/h speed with a WF5 defect on the left wheel (orange) compared to the NO DEFECT right wheel (blue), and (b) effect of down-sampling: original signal from a WF5 simulation at 300 km/h (blue) compared with its down-sampled version at 800 Hz (red)

Table 2. Numerical simulations: synthesis of the results computed on the vertical acceleration signals

Defect name	Speed (km/h)	RMS[1] (*g*)	Peak (*g*)	CF[2] (*g*)	Peak duration (ms)	Minimum f_{samp} (Hz)
	100	0.28	1.25	5.25	–	–
No defect	200	0.66	2.76	4.16	–	–
	300	1.22	5.23	4.30	–	–
	100	0.37	8.09	21.90	0.08	12,500
WF1	200	0.92	19.93	21.74	0.07	14,286
	300	1.50	32.51	21.65	0.04	25,000
	100	–	–	–	–	–
WF2	200	–	–	–	–	–
	300	–	–	–	–	–
	100	0.36	4.85	13.44	0.28	3,571
WF3	200	0.97	12.35	12.71	0.17	5,882
	300	1.60	22.13	13.80	0.14	7,143
	100	0.49	7.36	14.92	0.28	3,571
WF4	200	1.22	18.61	15.22	0.17	5,882
	300	1.92	31.84	16.57	0.15	6,667
	100	0.33	3.07	9.19	0.68	1,471
WF5	200	0.91	8.21	9.01	0.26	3,846
	300	1.59	15.96	10.05	0.20	5,000

Note: [1] Root mean square. [2] Crest factor.

RS. In this section, the test bench with the measuring set-up is described, along with the test schedule and the testing procedure adopted.

3.1. BU300 test bench

A picture of the BU300 test bench can be seen in Fig. 3. On the rig, a full-scale train wheelset is put in rotation by means of the contact with two disks with a 2 m diameter having a profile equal to the standard UIC60. The two disks are rigidly connected and driven by a DC motor, which allows a maximum peripheral speed of 300 km/h. A set of hydraulic actuators imposes the vertical (Q1 and Q2) and lateral (Y) load, and a set of electro-mechanical actuators is used for the lateral positioning of the wheelset with respect to the rail (Z1 and Z2) (see Fig. 3). The test bench can reproduce multiple conditions, constant speed, acceleration and braking, both on tangent tracks and in curved conditions. The BU300 full-scale roller rig has been extensively employed in previous investigations on railway dynamics. It has been used for calibrating instrumented wheelsets under realistic loads [41], reproducing near-service rolling contact fatigue conditions [42], optimizing actuator forces for accurate wheel–rail contact [43], and validating models for wheel wear prediction and derailment behaviour [44–46].

3.2. Experimental set-up

The tested wheelset had a nominal wheel radius of 0.46 m, and the vertical actuators Q1 and Q2 were set to +70 kN. Two tri-axial piezoelectric cabled accelerometers were cemented on a rigid support on top of the axle-boxes, thus on both the right and the left of the axle. The accelerometers model was 356A06, with a full scale of 500*g*: the three directions of interest (vertical, longitudinal and lateral) are thus acquired without saturation issues. BNC cables allow bringing the signal to an amplifier, from which the signal was acquired employing the National Instrument acquisition modules NI9234. The adopted sampling frequency ranged from 2.5 kHz to 25 kHz.

3.3. Test conditions

Railway wheelsets were tested in the conditions indicated in Tables 3 and 4. The wheel flats were artificially created through grinding processes.

Downloaded from https://academic.oup.com/tse/article/7/4/tdaf060/8362716 by Dipartimento di Elettronica/Informazione user on 06 March 2026

Fig. 3. The Lucchini RS BU300 full-scale roller rig

Table 3. Experimental tests of wheel-flat defects, with dimensions

Defect name	Length (mm)	Height (mm)	Distance (km)
WF1	10	2×10^{-2}	–
WF2	30	2×10^{-2}	–
WF3	30	5×10^{-2}	–
WF4	30	8×10^{-2}	–
WF5	60	8×10^{-2}	–
WF3+Wear 7	30	5×10^{-2}	12,200
WF5+Wear 7	60	8×10^{-2}	12,400

Table 4. Experimental tests of wear parameters

Defect name	Run distance (km)
No Defect	0
Wear 1	150
Wear 2	400
Wear 3	2,870
Wear 4	5,530
Wear 5	7,550
Wear 6	11,770
Wear 7	12,000

For wheel-flat investigation, seven different conditions were tested, listed in Table 3. Five of them are identified by the length and the width of the defect and have the same dimensions as the ones of the numerical simulations (Table 1). In the last two conditions, the wheel-flat defect has been coupled with the wear phenomenon; thus, the information regarding the kilometres run by the wheelset is added. From now on, wheel-flat test conditions will be described as WF, coupled with a number that identifies its increasing size. Two examples of a tested wheel-flat can be seen in Fig. 4.

A set of experimental tests was run on a healthy wheelset, allowing for gathering data where no defects are induced and only with increasing levels of run kilometres. These tests will

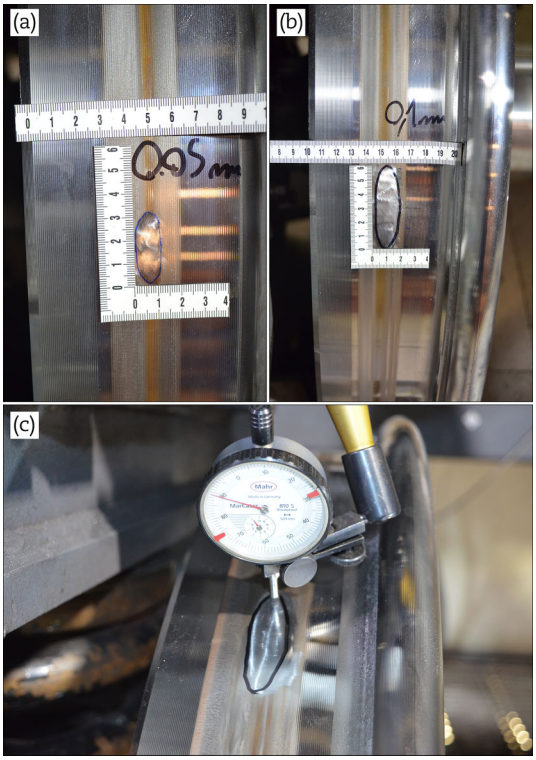

Fig. 4. Experimental tests pictures: (a) WF3 defect with length of 30 mm and approximate depth of 0.05 mm, (b) WF5 defect of length 60 mm and approximate depth of 0.1 mm, and (c) mechanical probe used for measuring defect depth

be addressed as Wear (Table 4), coupled with a number that identifies the increasing number of kilometres. The label No Defect refers to data collected from a brand-new wheelset, before any kilometres had been run. To ensure that the resulting wear conditions are as realistic and representative as possible, each test phase was preceded by running the wheelset along a mixed track composed of tangent sections and curves at various speeds, closely following the methodology adopted in previous studies [44, 45]. This approach, while not involving direct measurement of the wheel profile, aims to replicate the in-service evolution of wear through controlled but operationally relevant mileage accumulation.

For each condition, several speeds were tested in tangent track, from 50 km/h to 300 km/h, but the identification analysis will be showed in the following only: 100 km/h, 200 km/h and 300 km/h. Once the acquisitions were concluded, as mentioned before, the tests labelled WF2 were found damaged and were thus discarded and not processed.

4. Defect identification features

All vibration signals obtained during the tests are analysed through a specifically developed algorithm, and the conclusions extracted from the numerical simulations are tested on the new set of experimental data.

4.1. Raw data analysis

Wheel-flat data are analysed in the time domain. Fig. 5 presents vertical acceleration time histories corresponding to one second of acquisition under different wheel-flat conditions. Figs. 5(a) to (d) show the signals for the WF4 defect at 50 km/h, 100 km/h,

Downloaded from https://academic.oup.com/tse/article/7/4/tdaf060/8362716 by Dipartimento di Elettronica/Informazione user on 06 March 2026

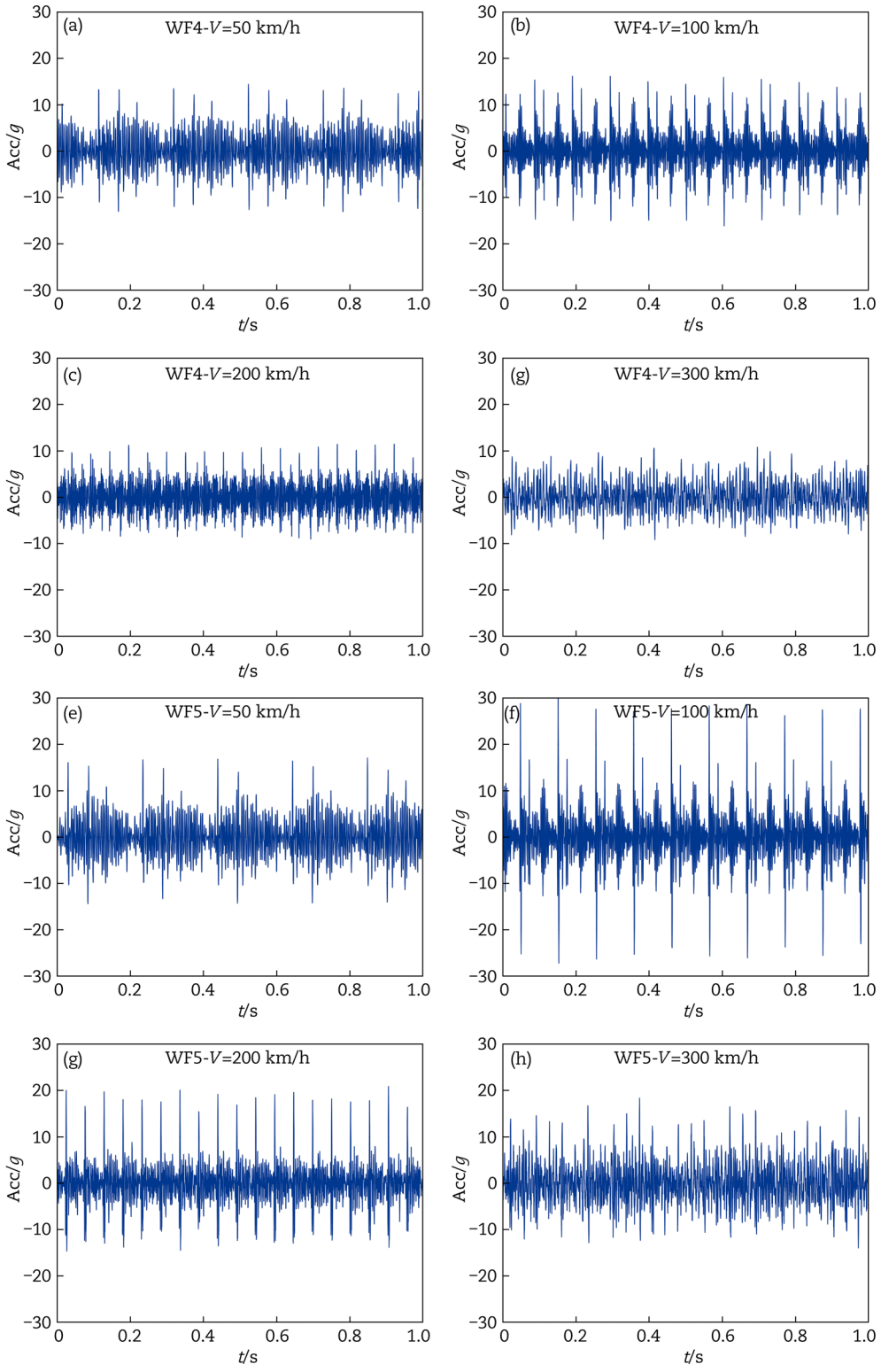

Fig. 5. Experimental tests, vertical ABA time histories over 1 s in the presence of wheel-flat defects: (a)–(d), WF4 at 50, 100, 200 and 300 km/h, respectively, and (e)–(h), WF5 at 50, 100, 200 and 300 km/h

200 km/h and 300 km/h, respectively, while Figs. 5(e) to (h) refer to the WF5 defect at the same speeds. In both cases, an increase in defect severity (from WF4 to WF5) at the same speed results in a noticeable increase in the amplitude of the acceleration peaks. Furthermore, speed itself exhibits a non-monotonic influence on peak amplitude: for each defect size, the amplitude increases from 50 to 100 km/h, but then decreases progressively at higher speeds, namely at 200 and 300 km/h. The found trend has already been discussed in published works, though in terms of wheel-rail contact force [47]. The study explores with numerical investigation wheel-flat induced peak wheel–rail contact forces from 0 to 400 km/h: the results show an in-

Downloaded from https://academic.oup.com/tse/article/7/4/tdaf060/8362716 by Dipartimento di Elettronica/Informazione user on 06 March 2026

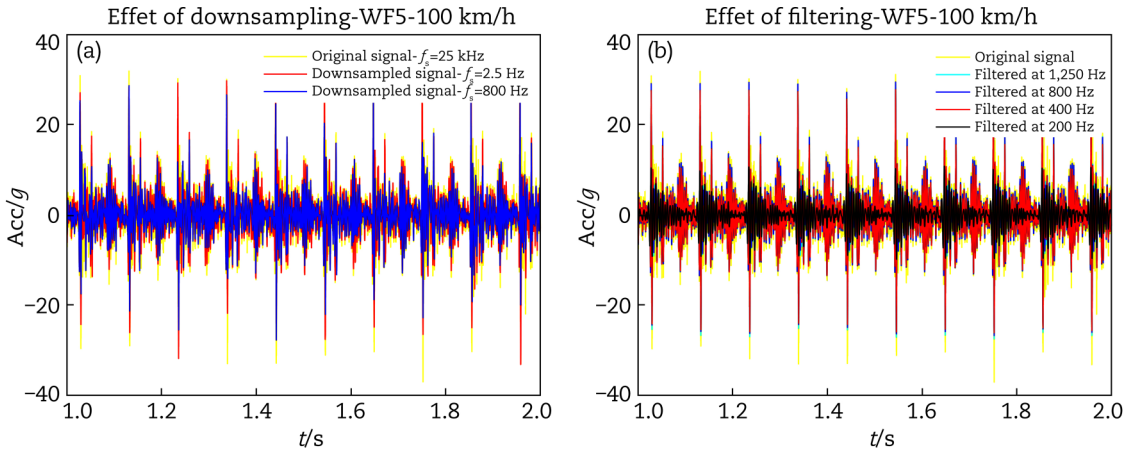

Fig. 6. Experimental tests, vertical ABA time histories over 1 second in the presence of WF5 defect at 100 km/h: (a) effect of downsampling, original signal at 25 kHz (yellow), downsampled at 2.5 kHz (red), and 800 Hz (blue), and (b) effect of low-pass filtering, original signal (yellow), filtered at 1.25 kHz (cyan), 800 Hz (blue), 400 Hz (red), and 200 Hz (black)

creasing trend of the latter with speed, reaching saturation at 100 to 120 km/h, followed by a decrease with further increase of the speed. Simulation results of Ref. [48] also confirm the same trends.

In any case, the signals suggest that low speed is more suitable to study wheel-flat effects on vibrational signatures.

The effects of filtering and downsampling are studied, for the sake of validating the outcomes of the numerical simulation results, to establish the minimum requirements for an on-board sensor acquisition for field data. WF5 at 100 km/h is considered as a sample case and a raw downsampling effect is obtained by applying a linear interpolation between the original signal, sampled at 25 kHz, and a time vector with a broader resolution. In Fig. 6(a), the acquisition, performed with a sampling frequency of 25 kHz, is compared with the same signal downsampled at 2.5 kHz and 800 Hz. By looking at these time histories, it is clear that in both cases it is possible to get at least one full peak in 1 s time history. Low-pass filtering is instead applied through a second-order Butterworth filter with different cut-off frequencies. The filtered signals are superimposed on the original time history in Fig. 6(b). The plot shows how using a cut-off frequency between 800 Hz and 1.25 kHz has a slight effect on peaks prominence, while filtering at 200 Hz has a huge effect on peaks reduction.

To sum up, a minimum sampling frequency of 800 Hz is required for any accelerometer sensor in the axle-box to measure impulses related to wheel flats, having care to use a cut-off frequency not lower than 400 Hz. This outcome validates the conclusions drawn from the numerical simulation (See Section 2.1.2), allowing the employment of a relatively low sampling frequency.

On the other hand, WF5 shows the highest values in terms of peak, with almost 30*g*, overturning the simulation results in Table 2. A full scale of at least 30*g* is thus needed to correctly sample a high wheel-flat dimension effect.

4.2. Features extraction

The following principle lays the foundation for features extraction on the acquired signals: the acceleration signal contribution related to the presence of the wheel-flat is periodic with the wheel revolution, i.e., all the information on the defect is present in the acceleration signal of a single wheel revolution. In a real case scenario, the same signal also contains components uncorrelated to the presence of the defect, e.g., track irregularities or impacts of insulated joints, that need to be filtered out. To do this, the knowledge of the rotational speed allows for cutting each acquisition into many sub-windows $1\times Rev$ period long, all correlated to one another. This allows building of a statistically significant dataset where a single event, as a joint impact, would be considered an outlier.

Firstly, data are pre-processed by downsampling at 2.5 kHz and are low-pass filtered according to the Nyquist principle, such as to simulate the acquisition of an on-board acceleration sensor.

Secondly, each acquisition is cut into windows a fundamental period long.

To do this, the wheel rotational frequency is identified by employing, with a slight modification, cepstral analysis, which is well described for railway application in the work of Baasch et al. [37] and carefully explained in Ref. [49]. Specifically, the power cepstrum is computed according to Eq. (6):

$$C_f(t) = \left|\mathcal{F}^{-1}\left(\log\left(\left|\mathrm{FFT}\left(ACF\right)\right|^2\right)\right)\right|^2, \tag{6}$$

where *ACF* is the autocorrelation function of the time acceleration signal. Thus, the cepstrum is the square of the inverse Fourier transform of the logarithm of the square of the power spectrum. The *ACF* signal allows for obtaining an attenuation of those components that are not periodic (such as noise or non-localized irregularities). Once the cepstrum of the *ACF* is computed, narrow peaks at frequencies multiple of the fundamental period are shown (see Fig. 7). The fundamental periodicity is found simply as the time instant at which the maximum peak in the cepstrum function occurs Eq. (7).

$$T_{1\times Rev} = \max(C_f(t)), \tag{7}$$

The algorithm is run independently on the three measured directions (longitudinal, lateral, and vertical), and the results are cross-checked to eliminate wrong identifications. For the specific case of these tests, the output of the cepstral analysis $f_{1\times Rev}$ (Eq. (8)) is accepted if lying within a ±5% interval with respect to the nominal frequency f_{nom} (Eq. (9)) used on the test bench acquisitions.

$$f_{1\times Rev} = \frac{1}{T_{1\times Rev}} \tag{8}$$

Downloaded from https://academic.oup.com/tse/article/7/4/tdaf060/8362716 by Dipartimento di Elettronica/Informazione user on 06 March 2026

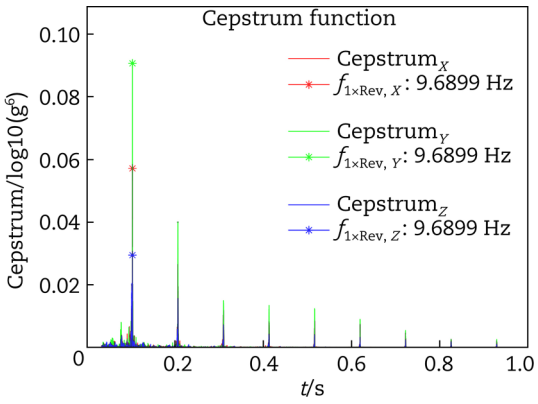

Fig. 7. Example of cepstrum analysis. Cepstrum function computed from the three-direction ABA signals of a test at 100 km/h with a WF5 defect

$$f_{\text{nom}} = \frac{V_{\text{nom}}}{2\pi \cdot 3.6 \cdot R} \tag{9}$$

In Eq. (9), R is the measured radius of the tested wheels (see Section. 3.2), whilst V_{nom} is the nominal linear speed in km/h. If the condition is verified, the results are averaged among the directions and the final value is assigned to the fundamental period. From a single acquisition, N_{wind} number of windows are cut, each of them containing the information about a single wheel revolution:

$$N_{\text{wind}} = \frac{T_{\text{tot}}}{T_{1\times Rev}}, \tag{10}$$

where T_{tot} is the time length of a generic test time history and $T_{1\times Rev}$ is the time length of the single window.

For each window, the following time features are computed.

- RMS. This shows the overall mean power of the signal.
- CF. This identifies peaks with respect to the RMS. Being a dimensionless index, it focuses on the identification of the shape of the signal itself regardless its amplitude.
- Wheel-flat severity index (WFI). This index allows quantification of the presence of peaks in the signal whilst keeping its dependence on the overall amplitude of the signal and peaks. It is a dimensional index firstly defined in Ref. [26] and follows Eq. (11).

$$WFI_W = \max(X_i) - RMS_W, \tag{11}$$

where W indicates the generic time window, X_i its relative time history and max is the maximum amplitude of the said window.

5. Results

Fig. 8(a) reports the statistical characterization of the three selected indicators—CF, WFI and RMS—for wheel-flat defects, across the three tested speeds: 100, 200 and 300 km/h. For each condition, the mean and standard deviation of the indicators are represented with error bars, providing insight into both central tendency and data dispersion. Fig. 8(b) presents the same statistical quantities for the datasets affected by profile wear, enabling an assessment of how wear influences the behaviour of each indicator.

The number of available samples used for the statistical computation is also shown in the first row of each figure. These values are critical to interpreting the reliability of the computed statistics, as they indicate the number of fundamental-period windows extracted from the acceleration signals under each condition. It is worth noting that the number of samples increases with speed, as higher train speeds result in a larger number of revolutions within the fixed time window used for signal acquisition. This increase in sample count contributes to reduced statistical uncertainty and better representation of the distribution for higher-speed datasets.

Additionally, it should be observed that the datasets for WF4 and WF5 contain a noticeably higher number of samples compared to the others. This is due to an update in the acquisition schedule, which allowed for more signal repetitions in these specific conditions. Despite the larger sample sizes, the associated standard deviations do not show significant deviations from the general trend, indicating a consistent feature behaviour and validating the comparability of these classes with the others.

From the statistical plots, several relevant observations can be made. First, the dispersion of the feature values—as indicated by the standard deviation—tends to increase with speed. This is particularly evident for the 300 km/h datasets, where all three indicators exhibit higher variability. This phenomenon can be attributed to increased dynamic complexity and greater sensitivity of the measurements to external perturbations at high speed (e.g., wheel-roller interaction noise).

Second, when analysing the wear datasets, a clear trend emerges. As the cumulative kilometres of operation increase—i.e., with increasing profile wear—there is a consistent rise in the RMS values of the vertical acceleration. A similar trend is observed in the WFI, likely due to its significant dependence on RMS. In contrast, the CF feature appears less sensitive to wear progression, showing only a slight decrease at 100 km/h, suggesting that it may be more effective in isolating localized defects such as wheel flats, rather than broader changes induced by wear.

The extracted features are inspected in two-dimensional plots: CF vs. RMS and WFI vs. RMS. Wheel-flat presence is tested by comparing the signals both in the complete absence of defects, i.e., the No Defect dataset, and in the presence of wear, i.e., the WEAR dataset (see Table 4).

Figs. 9(a) to (c) show the 2D features representation CF vs RMS, comparing the different levels of wheel-flat with the No Defect condition for each tested speed. In Figs. 9(d) to (e), the same plots are shown using the 2D feature plot representation WFI vs RMS.

A significant effect arises from the presence of WF. Both representations are able to catch a noteworthy difference between the No Defect and the most severe wheel-flat level. The effect of the presence of wear on wheel-flat identification is also investigated, by studying the trend of the Wear datasets. Figs. 10(a) and (b), show the 2D features representation CF vs. RMS and the WFI vs. RMS at one of the test case speed, 100 km/h. The plots compare the different levels of wheel-flat with the Wear condition, showing promising results for a clear distinction between the different datasets based on the selected features. The wear on the wheel profile has a considerable effect on the vertical acceleration RMS, as increasing level of wear leads to increasing RMS on the vertical acceleration, with a slight reduction of CF values.

To quantify the ability of each feature to properly distinguish between different defect levels and gain comprehensive conclusions, a pairwise overlap analysis was performed on the data distributions for each indicator. The goal of this analysis is to evaluate the separability of the classes by estimating how much the statistical distributions of different defect levels intersect.

Downloaded from https://academic.oup.com/tse/article/7/4/tdaf060/8362716 by Dipartimento di Elettronica/Informazione user on 06 March 2026

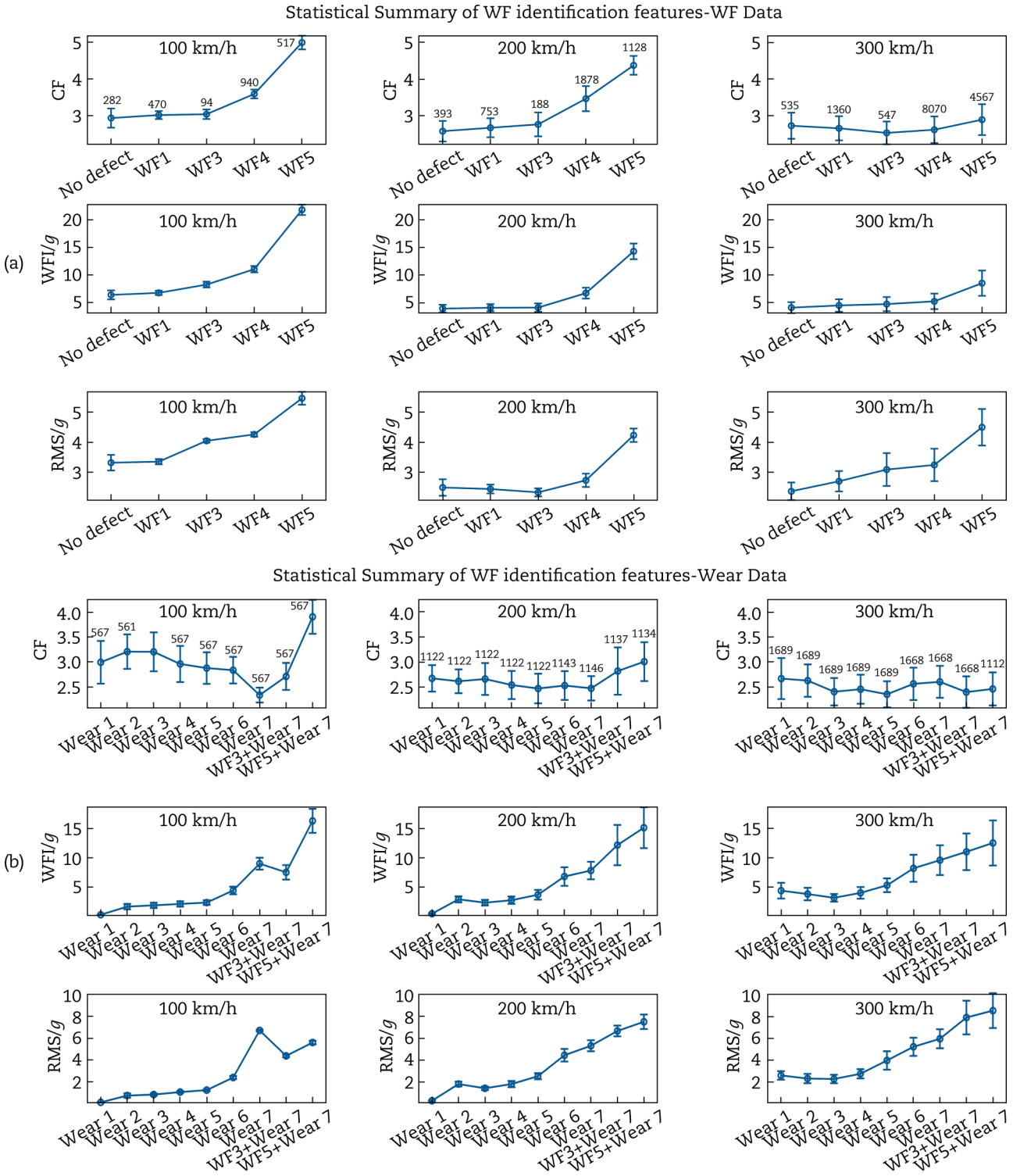

Fig. 8. Statistical analysis of time-domain indicators. Mean and standard deviation of CF, WFI and RMS values for different speeds and defect levels: (a) wheel-flat datasets at 100, 200 and 300 km/h, respectively, and (b) profile wear datasets. The number of samples used for each condition is indicated at the top of each plot

The methodology is based on non-parametric Kernel Density Estimation (KDE) to estimate the probability density function (PDF) of each defect class. For each pair of classes, the overlap coefficient was computed using the following definition:

$$Overlap = \int_{x_{common}} \min\left(f_1(x), f_2(x)\right) dx \tag{12}$$

where $f_1(x)$ and $f_2(x)$ are the estimated probability density functions of two defect classes, and x_{common} denotes the range over which both distributions are defined. The integrand $\min(f_1(x), f_2(x))$ captures the common area under the two curves at each point x. The resulting overlap coefficient ranges from 0 (no overlap, perfect separability) to 1 (complete overlap, no discriminative power). This metric offers an intuitive and quantitative way

Downloaded from https://academic.oup.com/tse/article/7/4/tdaf060/8362716 by Dipartimento di Elettronica/Informazione user on 06 March 2026

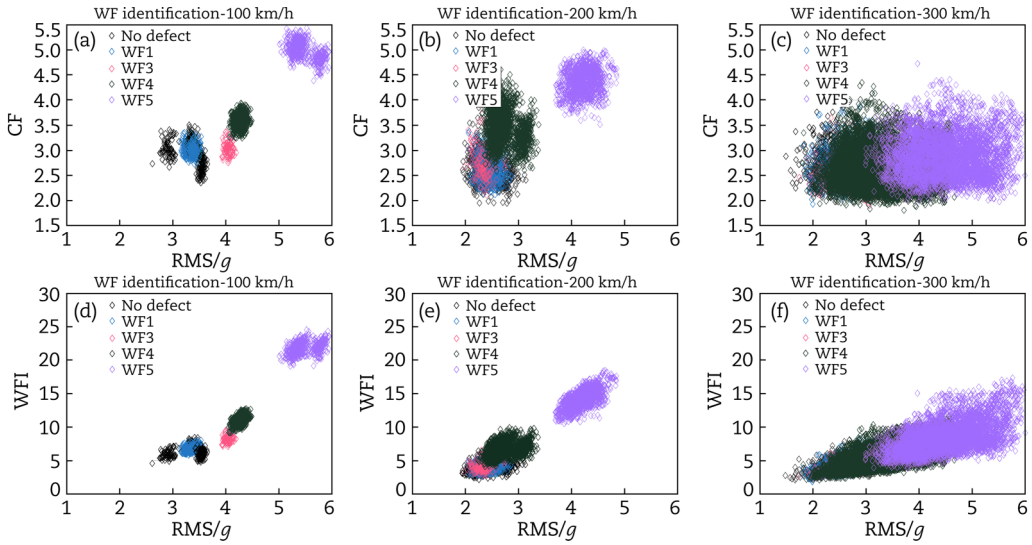

Fig. 9. 2D feature distribution at different speeds: (a) to (c) CF vs. RMS, and (d) to (f) WFI vs. RMS; (a) and (d) 100 km/h, (b) and (e) 200 km/h, (c) and (f) 300 km/h. Data points are coloured by defect level: black for No Defect, light blue for WF1, pink for WF3, green for WF4 and lilac for WF5. Each point corresponds to a feature value computed over a single wheel revolution

to assess the effectiveness of each feature in distinguishing between defect classes.

The results of this analysis are shown in Fig. 11, where subplots (a), (b) and (c) correspond to the overlap coefficients for the CF, WFI and RMS indicators, respectively. Each matrix plot displays the pairwise overlap coefficients between all defect classes, allowing direct comparison of the discriminative potential of each feature. Lower values in the overlap matrix suggest better separation and therefore higher diagnostic relevance.

The computed overlap coefficients offer a quantitative confirmation of the qualitative trends that can be observed in the feature spaces. Notably, the speed of 100 km/h consistently emerges as the most favourable operating condition for wheel-flat identification. At this speed, both WFI and RMS demonstrate excellent discriminative power: the overlap coefficient between WF4 or WF5 and the No Defect condition is effectively zero, indicating complete separability of these classes. Furthermore, the presence of wear does not significantly affect the feature distribution for these defect levels, confirming the robustness of the indicators under varying profile conditions. Even the WF3 level exhibits promising separability, with overlap values low enough to support reliable detection.

At 200 km/h, the performance of the features shows a moderate degradation. Only the most severe defects—WF4 and WF5—maintain a sufficiently low overlap with the No Defect class to allow for confident identification. For lower defect levels, increased data dispersion and reduced signal-to-noise ratio likely contribute to higher overlap values and lower discriminative capacity.

At 300 km/h, the identification capability further deteriorates. In this regime, only the most critical defect condition, WF5, remains clearly distinguishable from the healthy cases. The overlap coefficients for all other classes show substantial intersections, which compromise classification accuracy. These results align with the previously observed increase in feature variability at higher speeds and support the notion that low-speed acquisition is preferable for fault detection based on vertical ABA time indicators.

Additional insight is gained from the evaluation of compound defect conditions, where both wheel-flat and wear are simultaneously present. Specifically, the WF3 + Wear 7 and WF5 + Wear 7 cases were analysed. Results confirm that at 100 km/h and 200 km/h, the WF5 + Wear 7 condition remains clearly distinguishable from all No Defect and wear-only cases, demonstrating the resilience of the proposed features even under combined defect scenarios. This suggests that severe wheel-flat defects are identifiable regardless of advanced wear, at least up to moderate operating speeds. Conversely, for the WF3 + Wear 7 condition, some overlap persists, particularly at higher speeds.

Overall, WFI and RMS consistently outperform CF in terms of class separability across speeds and wear conditions. This confirms their suitability for robust wheel-flat detection, especially under low-speed operating regimes. At the same time, CF seems more insensitive to RMS variations. Indeed, Fig. 11(a) confirms how WF4 and WF5 show extremely low overlap with all No-defect conditions.

6. Discussion

The correct reproduction of the time profile of the impulse associated with each defect amplitude, thanks to the test bench, coupled with the carried-out analysis, allowed us to define correctly the needed specifics for an on-board vibration sensor for railway wheel-flat identification.

- A monoaxial vertical accelerometer can be sufficient for the identification of wheel-flats.
- By looking at Fig. 5(b), $\pm 50\,g$ can be considered a good choice for the full scale, as no more than $30\,g$ is measured also in WF5 condition.
- Real-scale experimental tests on a test bench confirmed that a minimum sampling frequency of 800 Hz is required for any accelerometer sensor in the axle-box to measure impulses related to wheel-flat presence.
- This study allows cutting each signal into fundamental-period long windows without the need for an encoder. This opens the possibility of designing a compact sensor easily fixable to the axle-box of a wheelset, without the need for further hardware and further energy consumption.

Downloaded from https://academic.oup.com/tse/article/7/4/tdaf060/8362716 by Dipartimento di Elettronica/Informazione user on 06 March 2026

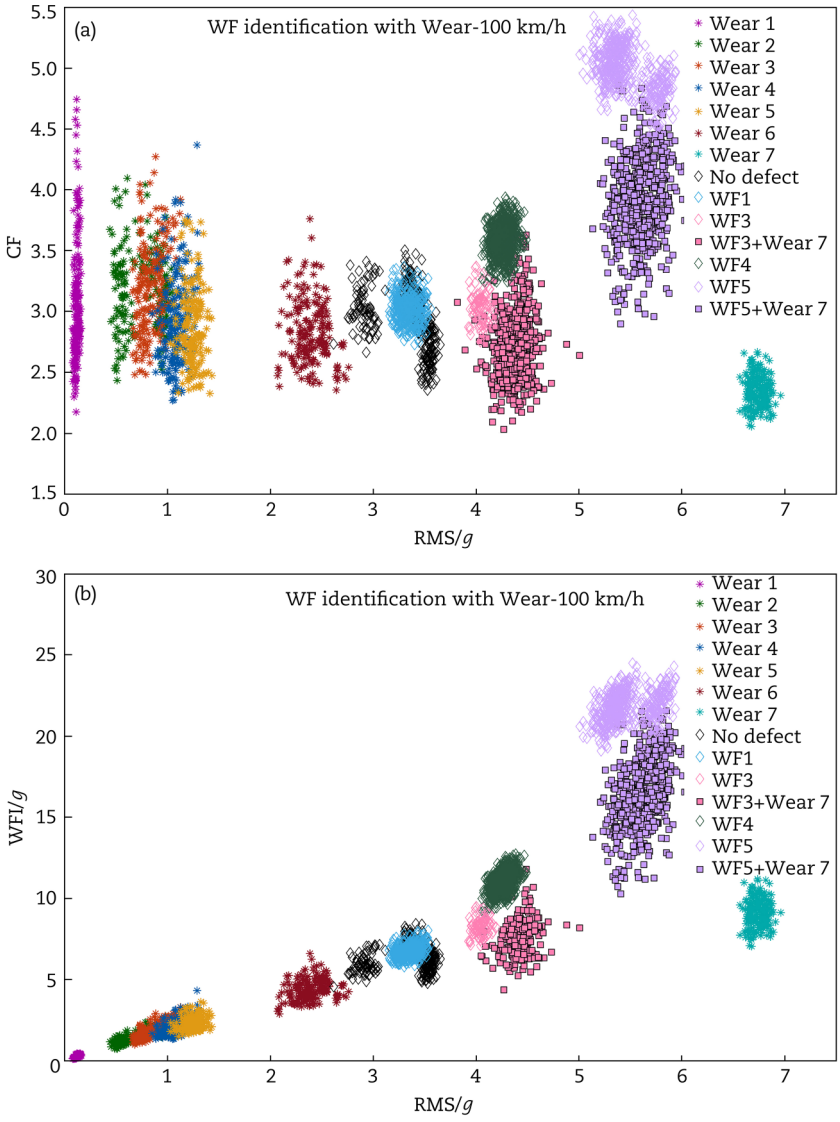

Fig. 10. 2D feature distribution at 100, km/h: (a) CF vs. RMS, and (b) WFI vs. RMS. Data points are colour-coded by condition: black for No Defect, light blue for WF1, pink for WF3, green for WF4 and lilac for WF5. Asterisks indicate measurements on nominal profiles; squares indicate measurements on worn profiles. Magenta, green, orange, blue, yellow, red and turquoise represent increasing wear levels (Wear 1 to Wear 7). Pink and lilac squares highlight WF3 + Wear 7 and WF5 + Wear 7 conditions, respectively. Each point corresponds to a feature value computed over a single wheel revolution

The conducted study presents a great number of advantages. The algorithm is straightforward to implement on a micro-controller, as it involves standard computational procedures. The developed approach greatly helps in significantly reducing the volume of the collected data (thus required memory storage) while preserving the features generated by the wheel-flat. For example, if we record vertical ABA at a sampling rate of 2.5 kHz over 10 s, we will gather 25,000 data points. By applying our method with a vehicle travelling at 100 km/h (where the wheel, with a 0.45 m radius, rotates approximately at 9.8 Hz, resulting in a rotation period of about 0.1 s), we obtain 100 windows for the signal. Consequently, we only require 300 data points (100 for RMS, 100 for CF and 100 for WFI) to accurately represent the original dataset. This reasoning point is also a great step towards a good low power consumption strategy, as the data transmission phase of an on-board sensor with a micro-controller has been proved by some of the authors in a previous work to be the most energy expensive [50]. The low power consumption holds great potential for advancing affordable and extremely energy-efficient sensor node systems, which are necessary for applications with a large number of sensors where electricity is not always available, such as freight trains.

As the time features are computed on windows a period of revolution long, the algorithm can effectively filter out outlier peaks not periodic with the wheel revolution, such as switches, crossing and insulated joints. Furthermore, the algorithm allows identification of WF of short dimension, particularly at 100 km/h, with 30 mm length, which becomes essential in terms of wheelset maintenance (see 1). This has also been proven possible in the presence of high levels of wear (12,000 km run).

Finally, we acknowledge that the developed algorithm still presents some challenges. It is designed to operate under stationary conditions, namely at constant vehicle speed. Testing on multiple wheel flats is required, as they tend not to present themselves regularly spaced around the wheel. On the contrary, periodic OOR possible presence is not going to influence the

Downloaded from https://academic.oup.com/tse/article/7/4/tdaf060/8362716 by Dipartimento di Elettronica/Informazione user on 06 March 2026

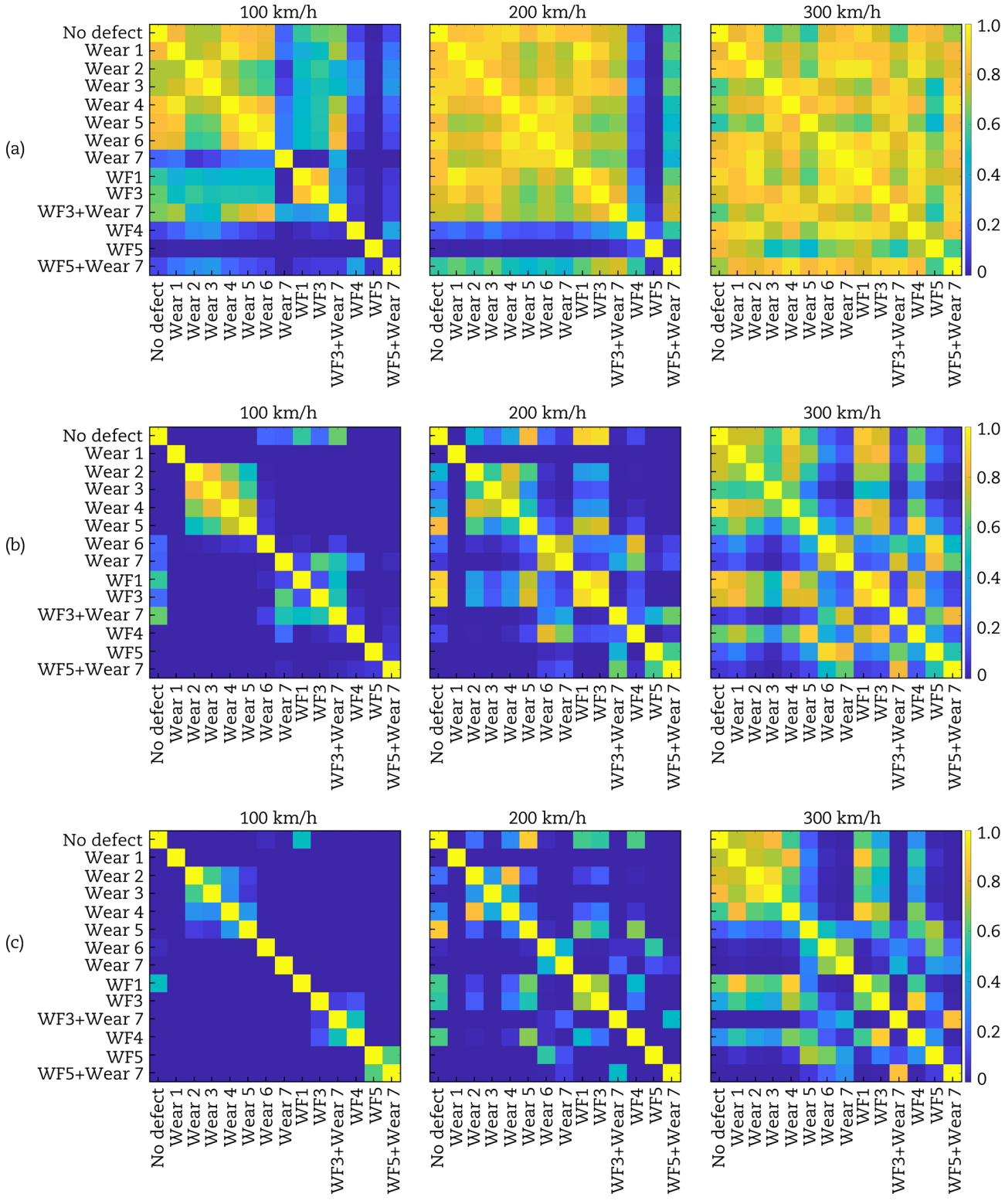

Fig. 11. Statistical overlap analysis. Pairwise overlap coefficients for: (a) CF, (b) WFI, (c) RMS. Colour scale: dark blue indicates no overlap (0), yellow indicates complete overlap (1)

algorithm identification, as it is typically detected through an order analysis in the frequency domain [1, 51–55]. While the presented results provide a reference under controlled conditions, the minimum identifiable wheel-flat severity may vary in field applications due to the presence of track irregularities, which are not replicated on the test bench. Further validation on field experimental campaigns is thus needed: monitoring of wheelsets in field conditions has already started [56] and focus on defects is planned for the following studies.

Moreover, the overlap-based analysis of feature distributions across various defect sizes, speeds and wear levels has shown the features' suitability for robust wheel-flat detection, especially

Downloaded from https://academic.oup.com/tse/article/7/4/tdaf060/8362716 by Dipartimento di Elettronica/Informazione user on 06 March 2026

under low-speed operating regimes, and provides a solid foundation for selecting and combining features in the development of automatic machine-learning-based classification algorithms.

7. Conclusions

In the present paper, an extensive study on the identification of railway wheelset wheel-flat from on-board ABA measurements was carried out. Starting from detailed numerical simulations with a multi-body model of a railway coach, a first estimate of how wheel-flat presence affects the wheels' dynamic response was accomplished. Time domain features were computed on numerical simulation results. The minimum sampling frequency and full scale, for an accelerometer of an on-board sensor, are estimated as a function of the wheel-flat severity.

Subsequently, experimental tests on a full-scale wheelset at the Lucchini RS BU300 test bench are described to validate the proposed algorithm based on time-domain feature extraction. Data obtained for different wheel conditions at different speeds are sampled, and the effect of filtering and downsampling is analysed on experimental data.

The time-domain features for the wheel-flat identification are extracted for each window of length equal to $T_{1\times Rev}$, cut from the original acquisition. To do this, the revolution speed is directly computed from the ABA signals through cepstral analysis, without the aid of any encoder. The identification of wheel-flat presence is investigated through two-dimensional feature plots—CF vs. RMS and WFI vs. RMS—as well as through an overlap-based analysis, which quantifies the separability of defect classes under different operational conditions. The comparison with No Defect data leads to the conclusion that WF4 and WF5 are easily distinguishable, especially at low speed, i.e., 100 km/h. The same analysis is carried out with the addition of the WEAR phenomenon. The latter, whilst significantly changing the results, let the condition WF5 still be detectable from the ones without defects.

In conclusion, the combined analysis of statistical distributions, feature space projections and pairwise overlap quantification demonstrates the diagnostic relevance of vertical acceleration-based indicators—particularly WFI and RMS—in detecting wheel-flat defects. These findings highlight the importance of acquisition speed in condition monitoring and confirm the potential of time-domain features for reliable, wear-resilient fault identification in railway systems.

This study builds the foundations for designing an on-board ABA measurements-based sensor for detecting railway wheel-flat. In a real case scenario, data coming daily from on-board sensors installed on a wheelset allows the creation of a solid database, which can be instrumental in the development of an automatic identification algorithm for condition monitoring and wheel-flat presence prediction. In this setting, the challenge will be the identification of new feature thresholds that can highlight the presence of the defect. Indeed, we expect the latter to be different from the ones found through test bench experimental tests, where the influence of train/track interaction, specific vehicle type and different load conditions is not present. For this, the integration of a tailor-made algorithm for the particular vehicle becomes essential.

Finally, as mentioned in the introduction, ABA measurements can be employed in the identification of further wheelset defects (axle crack, OOR, wearing phenomenon, etc.), thus this project opens the possibility of developing a complete low-power, compact on-board sensor for wheelset health diagnostics and defect identification.

Author contributions

Arianna Cavallo (Data curation, Formal analysis, Investigation, Software, Validation, Visualization, Writing–original draft, Writing–review & editing), Stefano Cii (Conceptualization, Formal analysis, Investigation, Methodology, Software), Gisella Tomasini (Conceptualization, Project administration, Supervision, Writing–review & editing), Francesco Castelli-Dezza (Project administration, Supervision), Steven Cervello (Resources), Daniele Regazzi (Resources).

Conflict of interest

The authors declared no potential conflicts of interest with respect to the research, authorship, and/or publication of this article.

References

1. Iwnicki S, Nielsen JCO, Tao G. Out-of-round railway wheels and polygonisation. *Veh Syst Dyn* 2023;**61**:1787–830.
2. Verband der Guterwagenhalter in Deutschland (VPI). *Maintenance of Freight Cars-Wheelsets*, 3rd Edition. Schauenburgerstraße. Hamburg, Germany, 2012.
3. Mercitalia Intermodal. Details obtained from a Private Interview on Maintenance Practice. 2024.
4. GCU Bureau (General Contract of Use for Wagons). *Technical Conditions for Wagon Transfers between Railway Undertakings*, Version: 1 January 2024. GCU Bureau, 2024.
5. Davari N, Veloso B, de Assis et al. A survey on data-driven predictive maintenance for the railway industry. *Sensors* 2021;**21**:5739.
6. Mobley RK. Impact of maintenance. In: *An Introduction to Predictive Maintenance*. Amsterdam: Elsevier; 2002, 1–22.
7. Binder M, Mezhuyev V, Tschandl M. Predictive maintenance for railway domain: a systematic literature review. *IEEE Eng Manag Rev* 2023;**51**:120–40.
8. Shaikh MZ, Ahmed Z, Chowdhry BS et al. State-of-the-art wayside condition monitoring systems for railway wheels: a comprehensive review. *IEEE Access* 2023;**11**:13257–79.
9. Alemi A, Corman F, Lodewijks G. Condition monitoring approaches for the detection of railway wheel defects. *Proc Inst Mech Eng Part F J Rail Rapid Transit* 2017;**231**:961–81.
10. Bernal E, Spiryagin M, Cole C. Onboard condition monitoring sensors, systems and techniques for freight railway vehicles: a review. *IEEE Sens J* 2019;**19**:4–24.
11. Ye Y, Li H, Wang Q et al. Fault diagnosis of railway wheelsets: a review. *Measurement* 2025;**242**:116169.
12. Nielsen JCO, Johansson A. Out-of-round railway wheels-a literature survey. *Proc Inst Mech Eng Part F J Rail Rapid Transit* 2000;**214**:79–91.
13. Wu TX, Thompson DJ. A hybrid model for the noise generation due to railway wheel flats. *J Sound Vib* 2002;**251**:115–39.
14. Iwnicki S. *Handbook of Railway Vehicle Dynamics*(1st Edition). CRC Press, 2006.
15. Jenkins H, Stephenson J, Clayton G et al. The effect of track and vehicle parameters on wheel/rail vertical dynamic forces. *Railway Engineering Journal* 1974;**3**.
16. Ye Y, Shi D, Krause P et al. Wheel flat can cause or exacerbate wheel polygonization. *Veh Syst Dyn* 2020;**58**:1575–604.
17. Dukkipati RV, Dong R. Impact loads due to wheel flats and shells. *Veh Syst Dyn* 1999;**31**:1–22.

Downloaded from https://academic.oup.com/tse/article/7/4/tdaf060/8362716 by Dipartimento di Elettronica/Informazione user on 06 March 2026

18. Jergéus J, Lundén R, Gullers P. Martensite formation around railway wheel flats. In: *Proceedings of the 11th International Wheelset Congress*, Paris, 1995;53–8.
19. Brizuela J, Fritsch C, Ibáñez A. Railway wheel-flat detection and measurement by ultrasound. *Transp Res Part C Emerg Technol* 2011;**19**:975–84.
20. Filograno ML, Corredera P, Rodríguez-Plaza M et al. Wheel flat detection in high-speed railway systems using fiber Bragg gratings. *IEEE Sens J* 2013;**13**:4808–16.
21. Liang B, Iwnicki SD, Zhao Y et al. Railway wheel-flat and rail surface defect modelling and analysis by time–frequency techniques. *Veh Syst Dyn* 2013;**51**:1403–21.
22. Liang B, Iwnicki S, Ball A et al. Adaptive noise cancelling and time–frequency techniques for rail surface defect detection. *Mech Syst Signal Process* 2015;**54/55**:41–51.
23. Chen S, Wang K, Chang C et al. A two-level adaptive chirp mode decomposition method for the railway wheel flat detection under variable-speed conditions. *J Sound Vib* 2021;**498**:115963.
24. Li Y, Liu J, Wang Y. Railway wheel flat detection based on improved empirical mode decomposition. *Shock Vib* 2016;**2016**:4879283.
25. Li Y, Zuo MJ, Lin J et al. Fault detection method for railway wheel flat using an adaptive multiscale morphological filter. *Mech Syst Signal Process* 2017;**84**:642–58.
26. Bosso N, Gugliotta A, Zampieri N. Wheel flat detection algorithm for onboard diagnostic. *Measurement* 2018;**123**:193–202.
27. Shim J, Kim G, Cho B et al. Application of vibration signal processing methods to detect and diagnose wheel flats in railway vehicles. *Appl Sci* 2021;**11**.
28. Bernal E, Spiryagin M, Cole C. Wheel flat analogue fault detector verification study under dynamic testing conditions using a scaled bogie test rig. *Int J Rail Transp* 2022;**10**:177–94.
29. Zhou Y, Tian Q, Hecht M. Wheel flat detection on railway vehicles using the angular domain synchronous averaging method: an experimental study. *Struct Health Monit* 2024;**23**:343–59.
30. Zhou Y, Vuitton J, Tian Q et al. Wheel flat detection by using the angular domain synchronous averaging method and axle box acceleration: simulation and experiment. *Measurement* 2024;**230**:114508.
31. UNI. EN 15313:2016 Railway applications-In-service wheelset operation requirements-In-service and off-vehicle wheelset maintenance. 2016.
32. Ye Y, Shi D, Krause P et al. A data-driven method for estimating wheel flat length. *Veh Syst Dyn* 2020;**58**:1329–47.
33. Ye Y, Wei L, Li F et al. Multislice time-frequency image entropy as a feature for railway wheel fault diagnosis. *Measurement* 2023;**216**:112862.
34. Bai Y, Yang J, Wang J et al. Intelligent diagnosis for railway wheel flat using frequency-domain gramian angular field and transfer learning network. *IEEE Access* 2020;**8**:105118–26.
35. Shi D, Ye Y, Gillwald M et al. Designing a lightweight 1D convolutional neural network with bayesian optimization for wheel flat detection using carbody accelerations. *Int J Rail Transp* 2021;**9**:311–41.
36. Ye Y, Huang C, Zeng J et al. Shock detection of rotating machinery based on activated time-domain images and deep learning: an application to railway wheel flat detection. *Mech Syst Signal Process* 2023;**186**:109856.
37. Baasch B, Heusel J, Roth M et al. Train wheel condition monitoring *via* cepstral analysis of axle box accelerations. *Appl Sci* 2021;**11**:1432.
38. Bruni S, Collina A, Diana G et al. Lateral dynamics of a railway vehicle in tangent track and curve: tests and simulation. In: *The Dynamics of Vehicles on Roads and on Tracks*. 2021, 464–77.
39. Fang W, Bruni S. A time domain model for the study of high frequency 3D wheelset–track interaction with non-Hertzian contact. *Multibody Syst Dyn* 2019;**46**:229–55.
40. ORE. B 176: *Bogies with Steered or Steering Wheelset, Report No.: Specifications and Preliminary Studies* , **Vol. 2**, *Specification for a Bogie with Improved Curving Characteristics*. Utrecht: ORE, 1989.
41. Jin X. Evaluation and analysis approach of wheel–rail contact force measurements through a high-speed instrumented wheelset and related considerations. *Veh Syst Dyn* 2020;**58**:1189–211.
42. Cantini S, Cervello S. The competitive role of wear and RCF: full scale experimental assessment of artificial and natural defects in railway wheel treads. *Wear* 2016;**366**:325–37.
43. Liu B, Bruni S. A method for testing railway wheel sets on a full-scale roller rig. *Veh Syst Dyn* 2015;**53**:1331–48.
44. Braghin F, Bruni S, Resta F. Wear of railway wheel profiles: a comparison between experimental results and a mathematical model. *Veh Syst Dyn* 2002;**37**:478–89.
45. Braghin F, Lewis R, Dwyer-Joyce RS et al. A mathematical model to predict railway wheel profile evolution due to wear. *Wear* 2006;**261**:1253–64.
46. Braghin F, Bruni S, Diana G. Experimental and numerical investigation on the derailment of a railway wheelset with solid axle. *Veh Syst Dyn* 2006;**44**:305–25.
47. Wu X, Rakheja S, Ahmed A et al. Influence of a flexible wheelset on the dynamic responses of a high-speed railway car due to a wheel flat. *Proc Inst Mech Eng Part F J Rail Rapid Transit* 2018;**232**:1033–48.
48. Wu TX, Thompson DJ. A hybrid model for the noise generation due to railway wheel flats. *J Sound Vib*. 2002;**251**:115–39.
49. Childers DG, Skinner DP, Kemerait RC. The cepstrum: a guide to processing. *Proc IEEE* 1977;**65**:1428–43.
50. Cii S, Tomasini G, Bacci ML et al. Solar wireless sensor nodes for condition monitoring of freight trains. *IEEE Trans Intell Transp Syst* 2022;**23**:3995–4007.
51. Chen S, Wang K, Zhou Z et al. Quantitative detection of locomotive wheel polygonization under non-stationary conditions by adaptive chirp mode decomposition. *Railw Eng Sci* 2022;**30**:129–47.
52. Wang Q, Xiao Z, Zhou J et al. A dynamic detection method for polygonal wear of railway wheel based on parametric power spectral estimation. *Veh Syst Dyn* 2023;**61**:2352–74.
53. Wang Q, Xiao Z, Zhou J et al. A new DFT-based dynamic detection framework for polygonal wear state of railway wheel. *Veh Syst Dyn* 2023;**61**:2051–73.
54. Song Y, Liang L, Du Y et al. Railway polygonized wheel detection based on numerical time-frequency analysis of axle-box acceleration. *Appl Sci* 2020;**10**.
55. Bruni S, Castelli-Dezza F, Cii S et al. Wireless sensor node for wheelset defects identification. In: *Proceedings of XIX International Wheelset Congress*. 2019:1–6.
56. Cavallo A, Bahgat M, Tomasini G et al. Procedure for wheel- flat identification on railway wheelset based on field and lab- oratory experimental tests. In: *Proceedings of the Sixth International Conference on Railway Technology: Research, Development and Maintenance* Edinburgh, UK, 2024.

Downloaded from https://academic.oup.com/tse/article/7/4/tdaf060/8362716 by Dipartimento di Elettronica/Informazione user on 06 March 2026

Received: April 14, 2025. **Revised:** September 17, 2025. **Accepted:** September 25, 2025
© The Author(s) 2025. Published by Oxford University Press on behalf of Central South University Press. This is an Open Access article distributed under the terms of the Creative Commons Attribution License (https://creativecommons.org/licenses/by/4.0/), which permits unrestricted reuse, distribution, and reproduction in any medium, provided the original work is properly cited.